Dynamical self-regulation in self-propelled particle flows

Arvind Gopinath, Michael F. Hagan, M. Cristina Marchetti, and Aparna Baskaran

Phys. Rev. E **85**, 061903 — Published 1 June 2012

DOI: 10.1103/PhysRevE.85.061903

Dynamical Self-regulation in Self-propelled Particle Flows

Arvind Gopinath[1], Michael F. Hagan[1], M. Cristina Marchetti[2] and Aparna Baskaran[1]
[1] *Martin Fisher School of Physics, Brandeis University, Waltham, MA, USA.*
[2] *Physics Department and Syracuse Biomaterials Institute, Syracuse University, Syracuse, NY 13244, USA.*

We study a continuum model of overdamped self-propelled particles with aligning interactions in two dimensions. Combining analytical theory and computations, we map out the phase diagram for the parameter space covered by the model. We find that the system self-organizes into two robust structures in different regions of parameter space: solitary waves comprised of ordered swarms moving through a low density disordered background, and stationary radially-symmetric asters. The self-regulating nature of the flow yields phase separation, ubiquitous in this class of systems, and controls the formation of solitary waves. Self-propulsion and the associated active convection play a crucial role in aster formation. A new result of our work is a phase diagram that displays these different regimes in a unified manner.

I. INTRODUCTION

Active fluids are comprised of interacting, self-propelled particles that individually consume energy and collectively generate large scale motion. Examples span many length scales, ranging from animal herds [1], schools of fish [2], bird flocks [3] and insect swarms [4], to bacterial colonies [5–7] and the cell cytoskeleton [8]. In this paper, we consider the overdamped dynamics of a collection of such particles subject to local aligning interactions. The model is relevant to various experimental systems, including motility assays [9], suspensions of cytoskeletal filaments [10], self-chemotactic bacteria such as E-coli in convection-free geometries [11], and inanimate systems such as vibrated granular monolayers [12] and chemically driven nano-rod suspensions [13].

The goal of our study is to identify universal hydrodynamic mechanisms for the emergence of complex structures in systems exhibiting collective motility. To this end, we focus on a simple yet generic macroscopic description in terms of a conserved density field and a collective velocity or polarization field. This mean-field model is expected to capture the behavior of the system on length scales large compared to the size of the individual units and on time scales long compared to the microscopic interaction times and the frictional relaxation times set by the medium. Such a description was first considered in the pioneering work of Toner and Tu [14–16] who found that self-convection inherent to active particle flows stabilizes long range order in two dimensions. Our study builds on this and related earlier works both analytically and numerically. Specifically, we map out emergent inhomogeneous structures, and identify the mechanisms underlying their formation.

The archetypal, overdamped self-propelled system we consider involves two parameters, the self-propulsion speed w_0 of the active particles and a parameter λ that incorporates the effect of non-linear inter-particle interactions. The theoretical model of Toner and Tu [14–16] yields a mean field transition from a disordered state to an ordered *polar* state (i.e., a state with nonzero mean velocity) that is controlled by the density of the active units. This density is not, however, an external control parameter as in conventional equilibrium phase transitions, but rather is convected by the order parameter. This coupling renders the dynamics of the system self regulating, in that the state of the system is determined by the interplay between particle convection and tendency to local alignment, rather than by an externally controlled density of active particles.

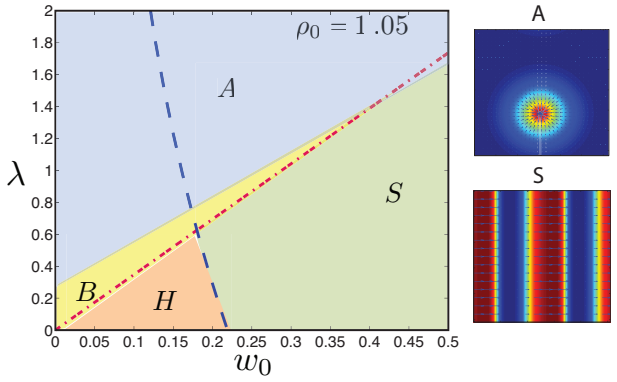

FIG. 1. (Color online) *Left Panel* : Phase diagram in the (λ, w_0) plane for $\rho_0 = 1.05$. The dashed (blue online) and dashed-dotted (red online) lines are the neutral stability curves for the L (Eq. (5)) and T (Eq. (6)) modes, respectively. The shaded regions describe the stable states obtained numerically: a homogenous polar state (H), a regime of propagating solitary stripes (S), a regime of stationary asters (A), and moving localized polar clusters (B). The domain size is (in dimensionless units) 128×128 and the equations were integrated up to 5×10^4 diffusion times. The moving polar clusters are a result of finite system size and the finite time of integration. *Right Panel*: Snapshot of a propagating stripe (bottom) and a stationary aster (top), the contours (color online - blue (low) and red(high)) denoting density.

Our main result is the phase diagram shown in Fig. 1, that displays the various dynamical states obtained by

varying w_0 and λ, for a fixed density above the mean-field order-disorder transition. As expected, the homogeneous polar state (H) is unstable in most of the parameter space. It is replaced by one of two robust structures in different regions of parameters. The first is a state of propagating solitary waves consisting of high density ordered swarms moving through a low density disordered background (see Fig. 1, Region (S)). The second is a stationary, radially-symmetric aster (see Fig. 1, Region (A)).

Density waves of the type found here are ubiquitous in bacterial systems [11, 17–22] and have also been observed in dense motility assays of short actin filaments [9]. Theoretical studies showing the emergence of traveling wave structures have included diffusion models with chemotactic gradients [23–26], numerical simulations of agent based models, such as the Vicsek model [27] and coarse grained theories [28–30]. In particular, Bertin et al [29] have recently pointed out that the traveling density stripes are solitary waves, rather than a nonequilibrium pattern of the system. In this work, we demonstrate that these density waves are an inevitable consequence of the self-regulating nature of self-propelled particle flows and can be viewed as a coexistence between two stable phases of the system, namely a high density ordered swarming state and a low density disordered state.

The other structure we find - asters - are ubiquitous in cell biology in processes such as the formation of the mitotic spindle [31, 32]. They also occur in *in-vitro* suspensions of cytoskeletal filaments and motor proteins [10, 33, 34]. Theoretical models of mixtures of cytoskeletal filament and motor proteins do indeed yield aster formation [35–39, 41, 42], arising from the dynamics of the motor proteins and/or the flow of the solvent. Asters have not, however, been obtained before in Toner-Tu continuum models of self-propelled particles because they only occur for stronger effective nonlinearities than considered in previous studies. In addition, our analysis identifies a universal hydrodynamic mechanism for aster formation in the change in sign of the effective nonequilibrium compressibility of the system, combined with the active self convection.

The layout of this paper is as follows. First, we review the hydrodynamic theory and describe the key features that control the emergent structures. Then, we carry out a linear stability analysis of the homogeneous swarming state and identify the mechanisms leading to onset of inhomogeneous structures. Next, we report the results of a numerical solution of the nonlinear deterministic equations and discuss the mechanisms underlying the formation of the propagating density waves and stationary asters. Finally, we conclude with a discussion that places our work in the context of the existing vast literature on active polar fluids.

II. THE CONTINUUM MODEL

We model the overdamped dynamics of a collection of self-propelled particles. The only conserved field is the number density $\rho(\mathbf{r},t)$ of active particles. In addition, to describe the possibility of states with polar orientational order or collective motility, we consider the dynamics of a vector field, $\boldsymbol{\tau}(\mathbf{r},t) = \rho(\mathbf{r},t)\mathbf{P}(\mathbf{r},t)$, that represents a polarization density. Here, $\mathbf{P}(\mathbf{r},t)$ is an order parameter for polar orientational order. Its magnitude measures the amount of orientational order and its direction represents the Goldstone mode associated with the spontaneously broken rotational symmetry in the swarming state. The dynamical equations associated with these quantities were first constructed phenomenologically by Toner and Tu [14] and have more recently been derived by coarse-graining various microscopic models [28, 29, 38, 41, 43, 44]. They are given by

$$\partial_t \rho = -\boldsymbol{\nabla}\cdot(w_0\boldsymbol{\tau} - D\boldsymbol{\nabla}\rho)\ , \tag{1}$$

$$\begin{aligned}\partial_t\boldsymbol{\tau}+\lambda_1(\boldsymbol{\tau}\cdot\boldsymbol{\nabla})\boldsymbol{\tau} = &-\left[a_2(\rho)+a_4|\boldsymbol{\tau}|^2\right]\boldsymbol{\tau} + K\nabla^2\boldsymbol{\tau}\\ &-w_1\boldsymbol{\nabla}\rho + \frac{\lambda_3}{2}\boldsymbol{\nabla}|\boldsymbol{\tau}|^2 + \lambda_2\boldsymbol{\tau}(\boldsymbol{\nabla}\cdot\boldsymbol{\tau})\ .\end{aligned} \tag{2}$$

The density equation, Eq. 1, is a conservation law with a mass flux controlled by the sum of convection of the active particles at the self-propulsion speed w_0 and diffusion at rate D. The structure of the polarization equation, Eq. 2, reflects the fact that $\boldsymbol{\tau}$ plays a dual role: on one hand $\boldsymbol{\tau}/\rho$ is the orientational order parameter of the system, on the other $w_0\boldsymbol{\tau}/\rho$ represents the mean flow velocity. The first two terms on the right hand side of Eq. 2 control the mean-field continuous order-disorder transition to a state of collective motility, with $a_2(\rho)$ a parameter that changes sign at a characteristic density ρ_c, and $a_4(\rho) > 0$. The term proportional to λ_1 describes self-convection. One may consider this as the active analog of the finite Reynolds number convective nonlinearity in the Navier-Stokes equation.

We note that the overdamped system just described does *not* possess Galileian invariance as the active particles move relative to the (damping) medium. As a result, $\lambda_1 \neq 1/\rho$. This lack of Galileian invariance also allows for other convective terms proportional to λ_2 and λ_3 that appear on the right hand side of the equation. In contrast however to the term proportional to λ_1, these terms also have an equilibrium interpretation and can be present in an equilibrium polar or ferroelectric fluid [45]. The term proportional to w_1 is essentially a pressure gradient and is unique to systems with polar symmetry.

Before proceeding further we point out the two crucial properties of the above equations that control the formation of emergent structures in this system.

(1) Dynamical Self-regulation. It is useful to compare Eq. 2 to that for the order parameter of an equilibrium lyotropic polar liquid crystal such as a smectic C Langmuir monolayer [46]. The important difference

is that in the equilibrium system the density controlling the order-disorder transition is externally tuned. In the case of a collection of self-propelled particles, the density is *convected by the order parameter* itself through the w_0 term in Eq. 1. In this sense the amount of order is regulated by the dynamics of the system and, critically, this coupling is rendered non-local by the convective terms. This is a crucial feature of the dynamics of self-propelled systems and plays a central role in controlling the formation of emergent structures.

(2) Negative effective compressibility. Two terms on the right hand side of Eq. 2 that are along the direction of the spatial gradient, namely $w_1\boldsymbol{\nabla}\rho - \frac{\lambda_3}{2}\boldsymbol{\nabla}|\boldsymbol{\tau}|^2$ represent pressure gradients, with $w_1\rho - \frac{\lambda_3}{2}|\boldsymbol{\tau}|^2$ the effective pressure. Although in general one could imagine a more complicated dependence of the effective pressure on density ρ and magnitude of polarization $|\boldsymbol{\tau}|$, the form chosen here has been obtained in a number of derivation of the continuum equations from microscopic models of self-propelled particles (see [29, 30] and references therein). The first term is the ideal gas part of the pressure. The second term arises due to the intrinsic tendency of polar systems to splay [45]. For $\lambda_3 > 0$, as obtained from all microscopic derivations [29, 30], it describes a lowering of the pressure due to ordering of the velocities. When λ_3 becomes large the system develops an effective negative compressibility. This central property controls the physics in the interaction dominated regime.

Given the large number of parameters in the hydrodynamic equations, Eq. 1 and 2, we now proceed to simplify them as follows. We choose $a_2 = \nu\,(1-\rho/\rho_c)$ and $a_4 = \left(\nu/\rho^2\right)(1+\rho/\rho_c)$, with ν being a characteristic kinetic frequency. These choices yield a continuous mean-field phase transition from an isotropic ($\boldsymbol{\tau} = \mathbf{0}$) to a homogeneous, polar or swarming state ($|\boldsymbol{\tau}| > 0$) at the critical density $\rho = \rho_c$ and ensures that $|\tau|/\rho \to 1$ for $\rho \gg \rho_c$. We further assume $D = K$ and measure time in units of ν^{-1} and lengths in units of $(D/\nu)^{\frac{1}{2}}$. Without loss of generality, we also set the critical density $\rho_c = 1$. To further reduce the number of independent parameters, computations are carried out for $w_1 = w_0$ and $\lambda_1 = \lambda_2 = \lambda_3 = \lambda$. This minimal choice is consistent with systematic derivations of these equations from physical microscopic models [29, 43, 44]. The simplified equations then involve just three parameters: (1) the mean density of the system, ρ_0, which determines the distance from the order-disorder transition, (2) the convective velocity w_0, and (3) λ which is controlled by the strength of interparticle interactions. The hydrodynamic equations in dimensionless simplified variables are given by

$$\partial_t\rho = -\boldsymbol{\nabla}\cdot(w_0\boldsymbol{\tau} - \boldsymbol{\nabla}\rho)\,, \tag{3a}$$

$$\partial_t\boldsymbol{\tau} = -(a_2 + a_4\boldsymbol{\tau}^2)\boldsymbol{\tau} - w_0\boldsymbol{\nabla}\rho + \nabla^2\boldsymbol{\tau} + \lambda\left(\tau_\alpha\boldsymbol{\nabla}\tau_\alpha + \boldsymbol{\tau}\boldsymbol{\nabla}\cdot\boldsymbol{\tau} - \boldsymbol{\tau}\cdot\boldsymbol{\nabla}\boldsymbol{\tau}\right)\,, \tag{3b}$$

where w_0 and λ are now dimensionless.

III. LINEAR STABILITY ANALYSIS

In this section, we examine the linear stability of the homogeneous solutions to Eqs. (1) and (2). We use dimensionless variables in our analysis, but to highlight the role of each term in the complete hydrodynamic equations, we allow for the parameters w_0, w_1, λ_1, λ_2 and λ_3 to have different values.

The continuum equations (1) and (2) have two homogeneous, stationary solutions, both with $\rho = \rho_0 =$ constant: an isotropic state with $\boldsymbol{\tau} = 0$ for $\rho_0 < \rho_c \equiv 1$ and a polar state with $\boldsymbol{\tau} \neq 0$ for $\rho_0 > \rho_c$. We focus here on the polar (or collective motile) state. Without loss of generality, we take the direction of polarization to be the x axis of our coordinate system. The homogeneous polar state is then characterized by $\boldsymbol{\tau} = \tau_0\hat{\mathbf{x}}$ with $\tau_0 = \rho_0\sqrt{(\rho_0-\rho_c)\,/\,(\rho_0+\rho_c)}$.

The stability of this homogeneous state to small amplitude perturbations $\rho = \rho_0 + \delta\rho\,(\mathbf{r},t)$, $\boldsymbol{\tau} = \boldsymbol{\tau}_0 + \delta\tau\,(\mathbf{r},t)\,\hat{\mathbf{x}} + \delta\tau_\perp\,(\mathbf{r},t)\,\hat{\mathbf{y}}$ may be readily examined. Introducing the Fourier representation $\widetilde{x}\,(\mathbf{q},t) = \int d\mathbf{r}e^{i\mathbf{q}\cdot\mathbf{r}}x\,(\mathbf{r},t)$, we obtain the linearized equations

$$\partial_t\delta\widetilde{\rho} = -q^2\,\delta\widetilde{\rho} + iw_1(q_\parallel\,\delta\widetilde{\tau} + q_\perp\,\delta\widetilde{\tau}_\perp)\,, \tag{4a}$$

$$\partial_t\delta\widetilde{\tau} = (\alpha_1 + iw_1q_\parallel)\,\delta\widetilde{\rho} - (\alpha_2 + i\overline{\lambda}\tau_0q_\parallel + q^2)\,\delta\widetilde{\tau} - i\lambda_2\tau_0q_\perp\,\delta\widetilde{\tau}_\perp\,, \tag{4b}$$

$$\partial_t\delta\widetilde{\tau}_\perp = iw_0q_\perp\,\delta\widetilde{\rho} - i\lambda_3\tau_0q_\perp\,\delta\widetilde{\tau} + (i\lambda_1\tau_0q_\parallel - q^2)\,\delta\widetilde{\tau}_\perp\,, \tag{4c}$$

with $\overline{\lambda} = \lambda_3 + \lambda_2 - \lambda_1$, $q_\parallel = q\cos\theta$, $q_\perp = q\sin\theta$, θ being the angle between the wavevector $\mathbf{q}$ and the direction of broken symmetry, $\hat{\mathbf{x}}$ and the parameters $\alpha_1 \equiv -\tau_0\left(\frac{\partial a_2}{\partial\rho} - \frac{a_2^0}{a_4^0}\frac{\partial a_4}{\partial\rho}\right)$, and $\alpha_2 \equiv -2a_2^0$, with $\alpha_1 \geq 0$ and $\alpha_2 \geq 0$ for $\rho_0 > \rho_c$. We next seek solutions of the form $\delta\widetilde{\rho}, \delta\widetilde{\boldsymbol{\tau}} \sim e^{s_\alpha(\mathbf{q})t}$ so that the homogeneous state is stable only when $\mathrm{Re}[s_\alpha(\mathbf{q})] < 0$ for all eigenvalues. The details of the linear stability analysis have been discussed elsewhere [29, 30] and we will only provide a summary with focus on the aspects relevant to emergent structures. The physics is highlighted by examining the special cases of wavevector $\mathbf{q}$ along the direction of broken symmetry ($\theta = 0$) and in the normal direction ($\theta = \pi/2$).

Convection mediated density instability. When $\theta = 0$ and $q = q_\parallel$, the fluctuations $\delta\tau_\perp$ decouple and are always stable. The coupled equations for the density and magnitude fluctuations give the dispersion relations for the these two modes. In the long wavelength limit $q \to 0$ one finds that these modes are unstable provided

$$1 + \frac{w_0w_1}{\alpha_2} - w_0^2\frac{\alpha_1^2}{\alpha_2^3} - \overline{\lambda}\tau_0w_0\frac{\alpha_1}{\alpha_2^2} < 0\,. \tag{5}$$

The equations leading to (5) demonstrate that this instability is intimately related to the self regulating nature of the dynamics. It arises from the density dependence of the tendency of the system to build up polar order,

$a_2(\rho)$, and the fact that this density dependence is rendered nonlocal by the convective coupling of density to $\boldsymbol{\tau}$ proportional to w_0 and w_1. The location of the longitudinal instability line defined by Eq. (5) in the (λ, w_0) plane is shown by the dashed (blue online) line in Fig. 1 for a fixed value of density. Alternatively, one can identify a density $\rho_R(\lambda, w_0)$ such that magnitude fluctuations in the order parameter destabilize the homogeneous polar state for $\rho_R > \rho_c$, leading to the onset and growth of density inhomogeneities.This longitudinal instability has been previously identified in Refs. [29] and [30] and will be referred to here as the convection-mediated density instability. We want to emphasize two features of this instability: i) the mode is mainly controlled by the third term in Eq. (5) and as such is model independent. Furthermore, it arises purely due to the convective coupling between the collective velocity and density; ii) as the order-disorder transition is approached from above $\alpha_2 \to 0$ and $w_{0c} \sim (\rho_0 - \rho_c)^{\frac{1}{2}}$, i.e., near ρ_c the mean-field ordered state becomes unstable for vanishingly small w_0.

Splay induced negative compressibility. We now consider the dynamics of fluctuations in the direction orthogonal to the polarization, i.e., for $\theta = \frac{\pi}{2}$ or $q = q_\perp$. In this case the modes are all stable and diffusive near the isotropic-polar mean-field transition [30]. Far from the transition, fluctuations in $\delta\tau$ decay rapidly and can be eliminated in favor of $\delta\rho$ and $\delta\tau_\perp$ by using the quasi-steady approximation $\delta\tau \approx \left(\frac{\alpha_1}{\alpha_2}\right)\delta\rho - \left(\frac{iq\lambda_3\tau_0}{\alpha_2}\right)\delta\tau_\perp$. Substituting this expression in Eqs. (4a) and (4c) we find that $\delta\tau_\perp$ fluctuations - which in this case describe splay deformation of the order parameter - are unstable for

$$w_1 - \lambda_3\tau_0\frac{\alpha_1}{\alpha_2} < 0\,. \tag{6}$$

Note that this splay instability is controlled by the nonlinear coupling proportional to λ_3 and occurs when the effective compressibility of the system as determined by the third and fourth terms on the right hand side of Eq. (2) changes sign.The parameter λ_3 is in turn determined by interactions in the system [29, 30] and hence the precise location of the instability line is model dependent.

To summarize, we have identified two mechanisms that render the system linearly unstable and lead to growth of infinitesimal density fluctuations. In §III, we go beyond the linear stability analysis and use detailed numerical computations to characterize the spatially (and in certain cases temporally) inhomogeneous states that replace the homogeneous solution in the unstable region of parameters.

IV. EMERGENT STRUCTURES

To study the emergent structures arising from the nonlinear model, Eqs. (3a) and (3b) were solved numerically in two spatial dimensions using both an explicit (FTCS) scheme as well as a semi-implicit spectral

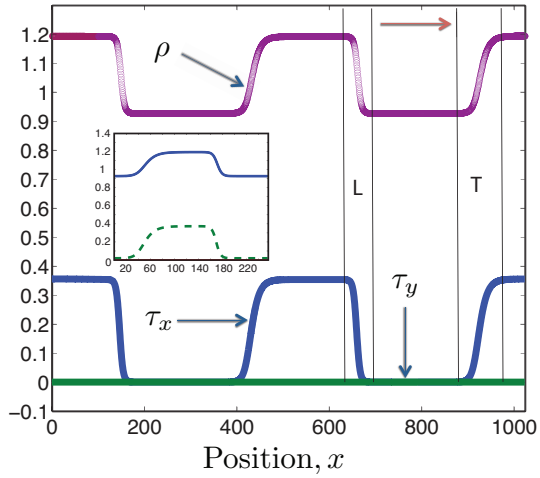

FIG. 2. (Color online) Profiles of ρ, the density (upper curve, pink in online version) and τ_x and τ_y the polarization fields (lower curves, blue and green online) are plotted for a striped state when $w_0 = 0.4$, $\lambda = 0$ and $\rho_0 = 1.05$. The system size is 1024×32 and results shown are obtained after integrating to 10^4 diffusion times. The arrow on the top right (red online) denotes the direction of motion of the stripes The vertical lines demarcate the trailing (T) and leading (L) edges of the stripe. The inset shows the details of the profile of density (solid line, blue online) and polarization (dashed line, green online) for one stripe.

Fourier-Galerkin scheme. In most calculations the system was started in a homogenous, non-polar (disordered) state, with small amplitude, uniformly distributed, zero-mean noise. Local initial density perturbations were chosen to be less than 3% of the mean density.

The results are summarized in the phase diagram shown in Fig 1 and discussed briefly in the introduction. For large values of activity the homogenous polar state (H) is unstable and two steady, inhomogeneous states are obtained: (i) propagating stripes comprised of ordered swarms moving through a disordered background, when active convection exceeds the strength of nonlinearities $w_0/\lambda \gg 1$, and (ii) a stationary aster when non-linear effects dominate convection $\lambda/w_0 \gg 1$. We now discuss the mechanisms underlying the formation of these two long-lived structures.

A. Solitary waves

We begin by considering the dynamics of the system in the convection dominated regime. For values of w_0 above the critical value for the onset of the convective density instability, defined by Eq. (5), an initially homogeneous state develops hot-spots of high density that are then convected throughout the system due to the coupling between $\boldsymbol{\tau}$ and ρ. These high density regions reorganize and grow in the direction lateral to their motion due to diffusion, resulting in the formation of high density, highly ordered planar stripes propagating at a speed of order w_0

through a low density, disordered background. We stress three striking properties of these stripes: i) they are not a pattern in that the width and spacing of the stripes is not fixed but rather determined by initial conditions and domain size - they are instead solitonic wavefronts; ii) the propagation speed c is of the order of w_0 and weakly dependent on the base density of the system; iii) The bands are bounded by two sharp fronts - a leading, narrow boundary layer and a wider and more slowly decaying trailing boundary layer (see Fig. 2). Similar stripes have been observed previously in discrete particle simulations as in [29].

Mechanism. Computations show that the propagating stripe state persists even when we set λ to zero. In addition, the onset of the striped state closely follows the neutral stability line associated with the convection mediated density instability determined by Eq. 5.

A minimum dynamical model for the emergence of this structure is given by the coupled equations $\partial_t \rho = -w_0 \partial_x \tau$ and $\partial_t \tau = -(a_2 + a_4 \frac{\tau^2}{\rho^2})\tau - w_0 \partial_x \rho$. These equations are equivalent to a wave equation where the homogeneous nonlinear terms from the polarization equation provide the dispersion that generates the solitary wave structure. After transforming to a co-moving frame, the equations can be reduced to quadrature to determine the speed of propagation and the profile of the wavefront. Such an analysis has already been reported in [29].

Here, we present a complementary point of view. As stated earlier, the convection mediated density instability occurs in the vicinity of ρ_c. The polar ordered state is re-stabilized at higher densities. In this unstable regime, the dynamics of the system essentially yields a phase separation into a high density ordered state and a low density disordered state, both of which are now stable (see Fig. 3). The degree of order in the stripe is precisely $\tau_h = ((\rho_h - 1)/(\rho_h + 1))^{\frac{1}{2}}$, i.e., the value predicted by the mean field theory for a state of density ρ_h. The propagating nature of the ordered state results in the robust concentration waves observed in the numerical solution. Interestingly, we note that phase separated structures are also observed in active nematic systems [47] which are also self-regulating in nature, although via mechanisms different from polar convection.

Experimental Realizations. Propagating concentrations waves have been observed in dense actin motility assays [9] and in self-chemotactic bacterial suspensions [11].

For the actin system, the numerical modeling described in Ref. [9] yielded the conclusion that local polar aligning interactions among the filaments are necessary for the emergence of the propagating waves. These interactions need not be medium mediated and could arise from the fact that aligned actin filaments have very anisotropic friction constants for sliding along the direction of alignment when compared to sliding against it [48]. This strongly suggests that the propagating waves seen in actin motility assays are indeed the propagating stripes obtained in the our model of polar self-propelled particles due to the dynamic self-regulation of the collective motility.

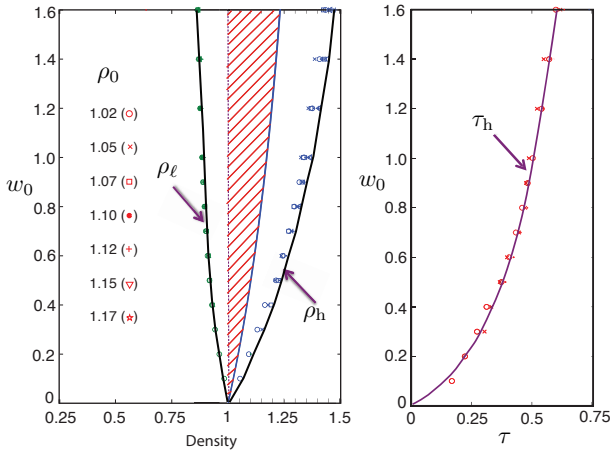

FIG. 3. (Color online) Illustration of the phase separation in the stripe state. *Left Panel*: Computational results obtained at $T = 10^4$ for a 128×128 domain with $\lambda = 0$. The shaded region (red stripes online) indicates the domain in parameter space when the polar state is unstable due to the convection mediated density instability. The density in the propagating stripe ρ_h and the low density background ρ_ℓ for various values of the base density and w_0 are shown. The lines are a guide to the eye. *Right Panel*: Plot of the polarization τ_h as a function of w_0 from the numerical simulation. The solid line is the analytical prediction $\frac{\rho_h(w_0)-1}{\rho_h(w_0)+1}$.

In contrast, patterns in bacterial suspensions are controlled by chemical and nutrient gradients and have been traditionally modeled using coupled reaction-diffusion equations. Recent work has shown that some patterns in chemotactic bacteria can be explained by accounting for the fact that the bacterial motility depends on density [49]. In the present context, we focus on the extensively studied *Keller-Segal bands* that are postulated to arise from self-chemotaxis and are the predominant emergent structure in convection free geometries [11]. The alignment interaction among bacteria in these systems scales with the concentration of the chemoattractant, which is in turn proportional to the concentration of bacteria. In this respect the alignment interaction is similar to the model considered here, where the local ordering tendency is controlled by a_2 which depends on the concentration of self-propelled particles. There is, however, an important difference between the two systems in that in the experiment of Ref. [11] and related studies, the direction of propagation of the bands is set by the nutrient gradient in the microchannel, hence the rotational symmetry is externally broken. In the model considered here, in contrast, the symmetry is broken spontaneously. However, we note that the fact that a symmetry is spontaneously broken is encoded in the dynamics of the associated Goldstone mode and the analysis here shows that the Goldstone mode plays no role in the dynamics that give rise to the concentration waves. Hence, the Keller-Segal bands

are also another realization of dynamic self-regulation in self-propelled particle flows.

B. Stationary Asters

We now focus on the other inhomogeneous stationary state obtained in the linearly unstable region of parameters, namely a stationary aster.

For $\lambda/w_0 \gg 1$ the numerical solution of the nonlinear equations yields asters or -1 topological defects with radially symmetric profiles of both density and orientational order. Stationary asters have been predicted using models with uniform density [35, 36], wherein the aster is strictly a defect in the order parameter. Here, it is also a region of high concentration.

A typical aster is depicted in Fig. 4. The density field ρ is a radially symmetric function of $r \equiv |\mathbf{r}|$ about the center of a -1 defect located for convenience at the origin of the coordinate system. The density is a maximum at $r = 0$ and decays exponentially far from the core to a value slightly below the critical density for the onset of ordering, $\rho_c = 1$. Unlike the density field, the order parameter, $\tau(r)$ is non-monotonic. Starting with a zero value at the core, the order parameter increases almost linearly to a intermediate maximum value $\tau_{\max}$ and decays exponentially to zero far from the aster's core. The point of maximum τ also corresponds to a point of inflection in the density profile.

We characterize the aster by two length scales, the size $\ell_{\rm co}$ of the aster core as defined as the distance from the aster's center to the point where $|\tau|$ reaches its maximum and the density has an inflection point, and the length scale ℓ_∞ characterizing the exponential decay of both density and polarization. This second length can be thought of as the size of the aster. Both length scales are only weakly dependent on the interaction strength λ for fixed w_0. For fixed λ we find that both $\ell_{\rm co}$ and ℓ_∞ decrease as a function of w_0 while the maximum density and the maximum τ increase. In other words, for fixed interaction strength, a larger self-propulsion speed yields denser, tighter asters. The behavior of density and the order parameter far form the center of the aster can be obtained from a simple asymptotic analysis of the dynamical equations as the nonlinearities do not play a significant role in determining the asymptotic behavior. Far from the core, assuming a radial dependence of both the density and the order parameter, and using the fact that $\tau \to 0$ at infinity, we can estimate the magnitude of the polarization by considering the steady state equation to linear order in small deviations from the asymptotic values $(\rho, \tau) = (\rho_\infty \leq 1, 0)$

$$r^2 \frac{d^2\tau}{dr^2} + r\frac{d\tau}{dr} - [r^2(1 - \rho_\infty + w_0^2) + 1]\tau = 0. \qquad (7)$$

The solution to the above equation is a Bessel's function of the second kind, that decays approximately as $e^{-\frac{r}{\ell_\infty}}$

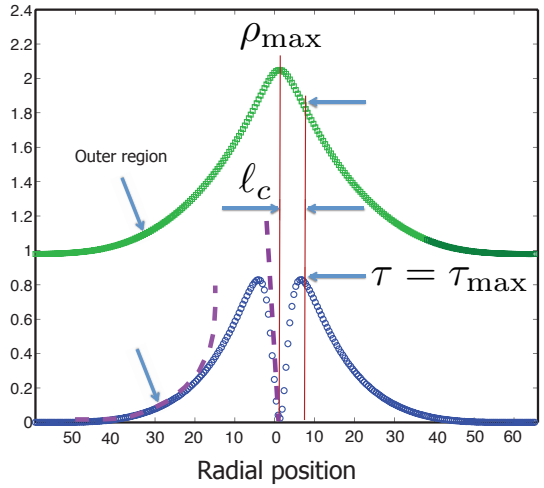

FIG. 4. (Color online) Radial density (top, green online) and $|\boldsymbol{\tau}|^2$ (bottom, blue online) profiles of an aster for $\rho_0 = 1.07$, $\lambda = 0.8$ and $w_0 = 0.05$. The system size is 128 x 128 and the equations have been integrated up to 10^4 diffusion times - these profiles remained constant even after integrating to 5 x 10^4 diffusion times. The density field $\rho(r)$ exhibits a point of inflection; at the same radial position the order parameter $|\boldsymbol{\tau}|$ attains a maximum value $\tau_{\max}$(indicated by the vertical lines). The aster is characterized by a core of size $\ell_{\rm co}$ and a region where both density and polarization decay over a characteristic length scale ℓ_∞. The dashed curves overlaying the lower figure of $|\boldsymbol{\tau}|^2$ are the theoretical result obtained by the asymptotic analysis based on Eq. (7) and described in the text.

with the length scale $\ell_\infty \sim (1 - \rho_\infty + w_0^2)^{-\frac{1}{2}}$, consistent with the trends identified in the numerical work. The behavior near the core is determined by a complicated interplay between the nonlinearities and cannot be investigated analytically.

Mechanism. The basic mechanism underlying aster formation is the splay-induced negative compressibility discussed in the context of the linear stability analysis. However, the self-regulating nature of the flow is critical for this instability as well since setting w_0 to zero does not yield any stable asters. We hypothesize that the system forms asters because this is the only steady structure that can accommodate the tendency to splay as well as to phase separate. Unlike the solitary wave discussed in the previous section, the aster state is however not a universal structure and depends on the values of the parameters in Eq. 2. The self-convection term (λ_1 in Eq. (2)) is critical for the formation of this structure. When we set this term to zero we find that the system develops streamers instead, a phase separated polar ordered state where, in contrast to the solitary wave state, the polarization is orthogonal to the direction of the spatial gradients (see Fig. 5).

Experimental Realizations. Aster formation has been seen in purified cell extracts of microtubules and associated motor proteins, such as those studied in Ref. [10, 33, 34]. In these controlled in vitro systems,

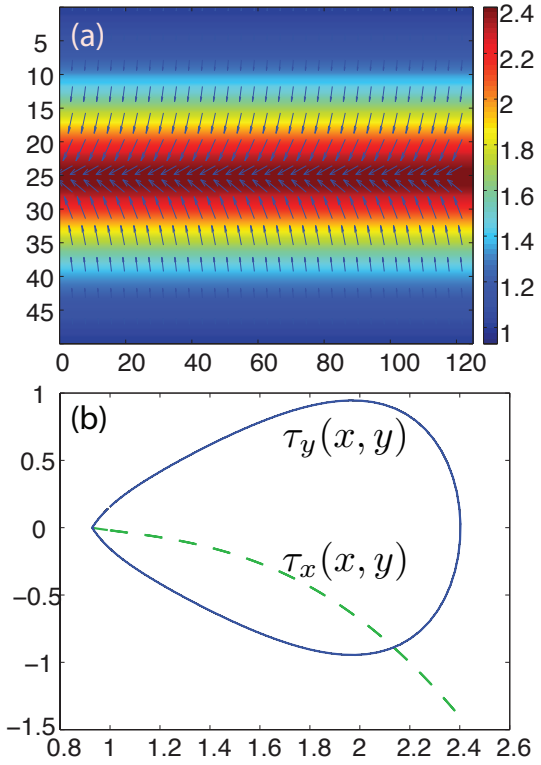

FIG. 5. (Color online) Steady inhomogeneous phase-separated structures which we term streamers, obtained at fixed domain size 128×128 when $\lambda_1 = 0$, $\lambda_2 = \lambda_3 = 0.8$, $w_0 = 0.1$ and $\rho_0 = 1.05$. The central high density (red online) region in (a) is also highly polar and ordered with the direction of polarity along the neutral direction. In (b) we quantify the polar variation by plotting the two components of $\boldsymbol{\tau}$ as a function of y. Note that τ_x (dashed line, green online) is a single valued function of y while τ_y (solid line, blue online) changes sign as we traverse the phase separated ordered region from one side to the other.

with known concentrations of only a few types of motor proteins, aster formation can be understood theoretically using both continuum models [35, 36, 38] and simulations [42]. Understanding the origin of aster-type structures in vivo, such as the formation and splitting of the mitotic spindle upon cell division, is much more challenging as in this case the process is controlled by a variety of competing nonequilibrium mechanisms, including microtubule polymerization and the on/off dynamics of many different motor types [31]. Our continuum theory where aster formation is controlled by only two competing parameters λ and w_0 may then guide the modeling and interpretation of these complex experiments. In particular, one can imagine fitting the spindle structure obtained in experiments on cells where various proteins have been systematically suppressed [31, 32] to our continuum model to identify which proteins directly affect the model's parameters and thereby back out the role played by the protein in the formation of the structure.

V. DISCUSSION

In this work, we have considered a generic continuum theory of self-propelled particles in the overdamped limit in two dimensions. An important new point of our work is the identification of dynamical self-regulation - the fact that the density that controls the amount of order is itself convected by the order parameter - as a crucial mechanism for the formation of emergent structures in these systems. We identify two robust structures in different regions of parameters: traveling solitary waves and stationary asters. We characterize these structures using numerical solutions of the deterministic nonlinear equations and identify the underlying hydrodynamic mechanisms associated with their emergence. The primary limitation of this study is that our system is overdamped or "dry". Momentum is not conserved and there is no coupling between polarization and actual flow. The "dry" system should be contrasted with an active polar suspension, consisting of active particles in a fluid that mediates hydrodynamic interactions. In the suspension the total momentum is conserved and important nonequilibrium effects arise from the coupling of the associated flow velocity and local orientational order, as shown in recent work [50, 51]. A second limitation is the one elastic constant approximation that identifies the energy cost for bend and splay. Theoretical work on models of suspensions of cytoskeletal filaments has shown the importance of retaining different elastic constants for bend and splay to understand the emergence of vortices and spirals [37, 52]. Future work will involve retaining the different elastic costs. Also, fluctuations play an important role in active systems. In this work fluctuations are introduced to ensemble averaged measurements through the stochastic initial conditions (and by numerical truncation errors). The influence of noise in the equations of motion on the robustness of emergent structures will be addressed in future work.

Finally, we note that aster formation has also been observed in related continuum models when the sign of pressure gradients tends to favor the formation of high density regions [38–40]. In particular, Gowrishankar and Rao [40] consider a model for active filaments without the self-regulation embodied in the density dependence of the coefficients a_2 and a_4 in Eq 3 and hence without the intrinsic tendency to phase separate. This model gives rise to arrays and lattices of asters. In contrast, asters were not found in Refs. [29, 30], even though the continuum equations considered there have the same structure as those analyzed here. The reason for this is that Refs. [29, 30] study the continuum model obtained by systematic coarse-graining of specific microscopic models (the Vicsek model and a collection of self-propelled hard rods, respectively) and use the microscopic expressions for the parameters obtained in such derivations. In both cases the microscopic calculation yields $\lambda \sim w_0^2$. In other words λ is not an independent parameter and cannot be tuned to the large values required to obtain asters.

The simplicity and generic nature of the theory considered in this study has enabled us to highlight the role of dynamic self regulation and to show that the mechanism is universal and does not depend on the microscopic physics, in contrast to closely related albeit system specific studies such as those in Refs. [39, 53].

Acknowledgements

AG, MFH and AB acknowledge support from the Brandeis-MRSEC through NSF DMR-0820492, and the HPC cluster at Brandeis for computing time. MCM was supported by the NSF on grants DMR-0806511 and DMR-1004789.

[1] J. K. Parrish and W. M. Hamner (eds), *Animal Groups in Three Dimensions*, Cambridge University Press (1997).
[2] S. Hubbard, P. Babak, S. Sigurdsson and K. Magnusson, Ecol. Model. **174**, 359 (2004).
[3] Physics Today **60**, 28 (2007); C. Feare, The Starlings, Oxford University Press (1984).
[4] E. Rauch, M. Millonas and D. Chialvo, Phys. Lett. A **207**, 185 (1995).
[5] C. Dombrowski, L. Cisneros, S. Chatkeaw, R. E. Goldstein and J. O. Kessler, Phys. Rev. Lett. **93**, 098103 (2004); A. Sokolov, I. S. Aranson, J. O. Kessler and R. E. Goldstein, Phys. Rev. Lett. **98**, 158102 (2007); E. Ben-Jacob, I. Cohen and H. Levine, Advances in Physics **49**, 395 (2000); B. M. Haines, I. S. Aranson, L. Berlyand and D.A. Karpeev, Phys. Biol. **5**, 046003 (2008).
[6] J. H. Kuner and D. Kaiser, J. Bacteriol. **151**, 458 (1982); M. S. Alber, M. A. Kiskowski and Y. Liang, Phys. Rev. Lett. **93**, 068102 (2004).
[7] X. -L. Wu and A. Libchaber, Phys. Rev. Lett. **84**, 3017 (2000); X. -L. Wu and A. Libchaber, Phys. Rev. Lett. **86**, 557 (2001).
[8] D. Mizuno, C. Tardin, C. F. Schmidt and F. C. MacKintosh, Science **315**, 370 (2007).
[9] V. Schaller, C. Weber, C. Semmrich, E. Frey, and A. R. Bausch, Nature **467**, 73 (2010).
[10] F. J. Nédélec, T. Surrey, A. C. Maggs and S. Leibler, Nature **389**, 305 (1997).
[11] Saragosti, J., Calvez, V., Bournaveas, N. et al., Proc. Natl. Acad. Sci. U.S.A , **108**, 16235 (2011).
[12] V. Narayan, S. Ramaswamy and N. Menon, Science **317**, 105 (2007); A. Kudrolli, G. Lumay, D. Volfson and L. S. Tsimring, Phys. Rev. Lett. **100**, 058001 (2008).
[13] W. F. Paxton et. al., J. Am. Chem. Soc. **126**, 13424 (2004); Y. Hong, N. M. K. Blackman, N. D. Knopp, A. Sen and D. Velegol, Phys. Rev. Lett. **99**, 178103 (2007).J. Palacci, C. Cottin-Bizonne, C. Ybert and L. Bocquet, Phys. Rev. Lett. **105**, 088304 (2010).
[14] J. Toner and Y. Tu, Phys. Rev. Lett. **75**, 4326 (1995).
[15] J. Toner and Y. Tu, Phys. Rev. E **58**, 4828 (1998).
[16] J. Toner, Y. Tu and S. Ramaswamy, Annals Of Physics **318**, 170 (2005).
[17] J. Adler, Science **153**, 708 (1966).
[18] S. Park, P. M. Wolanin, E. A. Yuzbashyan, et. al., Proc. Natl. Acad. Sci. U.S.A., **100**, 13910 (2003).
[19] H. Salman, A. Zilman, C. Loverdo, M. Jeffroy and A. Libchaber, Phys. Rev. Lett., **97**, 118101 (2006).
[20] G. Lambert, D. Liao and R. H. Austin, Phys Rev Lett **104**, 168102 (2010).
[21] M. J. Carlile, A. W. L. Dueney, B. K. Hebenstreit and R. H. Heerema, J. Magnetism and Magnetic Materials **67**, 291 (1987).
[22] N. H. Mendelson and J. Lega, J. Bacteriol., **180**, 3285 (1998).
[23] E. F. Keller and L. A. Segel, J. Theor. Biol., **26**, 399 (1970).
[24] M. P. Brenner, L. S. Levitov and E. O. Budrene, Biophys. J. **74**, 1677 (1998).
[25] M. J. Tindall, P. K. Maini, S. L. Porter, J. P Armitage, B. Math. Biol., **70**, 1570 (2008).
[26] J. Saragosti, V. Calvez, N. Bournaveas et. al., PLoS Comput. Biol., **6**, e1000890 (2010).
[27] G. Gregoire and H. Chate, Phys. Rev. Lett. **92**, 025702 (2004); H. Chate, F. Ginelli, G. Gregoire and F. Raynaud, Phys. Rev. E. **77**, 046113 (2008); F. Ginelli, F. Peruani, M. Bar and H. Chate, Phys. Rev. Lett. **104**, 184502 (2010).
[28] E. Bertin, M. Droz, and G. Gregoire, Phys. Rev. E **74**, 022101 (2006).
[29] E. Bertin, M. Droz and G. Gregoire, J. Phys A: Math. Theor. **42**, 445001 (2009).
[30] S. Mishra, A. Baskaran and M. C. Marchetti, Phys Rev E. **81**, 061816 (2010).
[31] T. U. Mayer, T. M. Kapoor, S. J. Haggarty et. al., Science **286**, 971 (1999); M. Shirasu-Hiza, Z. E. Perlman, T. Wittmann, E. Karsenti and T. J. Mitchison, Curr. Biol. **14**, 1941 (2004).
[32] S. C. Schaffner and J. V Jose, Proc. Natl. Acad. Sci. USA **103**, 11166 (2006); R. Loughlin, R. Heald and F. Nedelec, J. Cell. Biol., **191**, 1239 (2010)
[33] T. Surrey, F. Nedelec, S. Leibler and E. Karsenti, Science **292**, 1167 (2001).
[34] C. Hentrich and T. Surrey, J. Cell. Biol., **189**, 465 (2010).
[35] H. Y. Lee and M. Kardar, Phys. Rev. E **64,** 056113 (2001).
[36] S. Sankararaman, G. I. Menon, and P. B. Sunil Kumar, Phys. Rev. E **70**, 031905 (2004)
[37] R. Voituriez, J. F. Joanny, and J. Prost, Phys. Rev. Lett. **96**, 028102 (2006); K. Kruse, J. F. Joanny, F. Ju¨licher, J. Prost, and K. Sekimoto, Phys. Rev. Lett. **92**, 078101 (2004); K. Kruse, J. F. Joanny, F. Julicher, J. Prost, and K. Sekimoto, Eur. Phys. J. E **16**, 5 (2005)
[38] I. S. Aranson and L. S. Tsimring, Phys. Rev. E **74**, 031915 (2006).
[39] F. Ziebert, W. Zimmermann, Euro. Phys. J. E, **18**, 41 (2005).
[40] K. Gowrishankar and M. Rao, arXiv: 1201.3938
[41] T. B. Liverpool and M. C. Marchetti, Europhys. Lett. **89**, 846 (2005). T. B. Liverpool and M. C. Marchetti, Phys. Rev. Lett. **90**, 138102 (2003).
[42] E. Karsenti, F. Nédélec, T. Surrey, Nat. Cell. Biol., **8**, 1204 (2006).

[43] A. Baskaran and M. C. Marchetti, Phys. Rev. E. **77**, 011920 (2008); A. Baskaran and M. C. Marchetti, Phys. Rev. Lett. **101**, 268101 (2008).
[44] A. Ahmadi, M. C. Marchetti and T. B. Liverpool, Phys. Rev. E **74**, 061913 (2006).
[45] W. Kung, M. C. Marchetti, and K. Saunders, Phys. Rev. E **73**, 031708 (2006).
[46] P. G. de Gennes, *The Physics of Liquld Crystals*, Clarendon Press, Oxford (1995).
[47] S. Mishra and S. Ramaswamy, Phys. Rev. Lett., **97**, 090602 (2006).
[48] Z. Dogic, private communications.
[49] M. E Cates ME, D. Marenduzzo, I. Pagonabarraga, J. Tailleur, Proc. Natl. Acad. Sci. U.S.A **107**, 11715 (2010).
[50] S. M. Fielding, D. Marenduzzo, M. E. Cates, Phys. Rev. E, **83**, 041910 (2011).
[51] L. Giomi, L. Mahadevan, B. Chakraborty and M. F. Hagan, Phys. Rev. Lett., **106**, 218101 (2011); L. Giomi and M. C. Marchetti, Soft Matt., **8**, 129 (2012).
[52] K. Kruse, J. F. Joanny, F. Julicher, J. Prost, and K. Sekimoto, PRL 92 078101 (2004). K. Kruse, J. F. Joanny, F. Julicher, J. Prost, and K. Sekimoto, Eur. Phys. J. E **16**, 5 (2005).
[53] K. Doubrovinski and K. Kruse, Euro.Phys. J. E **31**, 95 (2010).